Sub-Micrometer Surface-Patterned Ribbon Fibers and Textiles

*Tural Khudiyev, Chong Hou, Alexander M. Stolyarov, and Yoel Fink**

The worldwide annual production volume of textiles is nearly one hundred million metric tons. Most of these undergo treatments to achieve specific properties, such as color, hydrophobicity, antimicrobial, or UV protection, using chemicals that lead to collateral environmental consequences. There is great interest in developing alternative and sustainable strategies to achieve textile functionality that do not involve chemical treatment. Here we present a thermal drawing approach to achieve fiber surface gratings on a rectangular cross-section. We demonstrate directional wetting properties as well as structural coloration based on the gratings. Periods down to ≈ 600 nm were established on the surface of a fiber. Fabrics displaying higher-order diffraction peaks in the visible regime were produced from surface-patterned fibers using convetional weaving machinery.

Presently, the worldwide annual production volume of textile fibers is nearly one hundred million metric tons.[1] Most of these fibers undergo chemical treatments to achieve properties, such as color, hydrophobicity, antimicrobial, UV protection, and others.[2–5] These chemical-based textile treatments come with significant societal penalties, including adverse health and environmental effects, as well as tremendous energy expenditures.[6–16] Therefore, alternative and sustainable strategies to achieve textile surface functionality are highly desired.

Here, we present a chemical-free approach that imparts specific optical and wetting properties to textiles based on thermal fiber drawing and surface patterning. To date, surface patterning of materials at the micro and nanoscales has been employed in diffraction gratings,[17] surface wetting,[18] plasmonic metasurfaces,[19] surface enhanced Raman scattering (SERS),[20] triboelectricity,[21] and biosurface interactions.[22] Various techniques,[23,24] including molding and embossing, masked deposition, optical lithography, e-beam lithography, and scanning probe techniques, have been developed for patterning at length scales ranging from nanometer to millimeter. Some work on texturing of fibers via thermal fiber drawing is also reported.[25] To impart specific functions to textiles, individual fibers need to be flexible and be produced at high-throughput, with uniform cross-sectional features at the micrometer or sub-micrometer scale. Here, we report on a two-step surface patterning technique called fiber surface patterning (FSP), based on a combination of macro-machining and thermal fiber drawing that enables high spatial resolution (sub-micrometer scale) patterning over kilometer-long lengths on flexible substrates, with high spatial uniformity (≈ 1%) and at speeds that are at least an order of magnitude faster than conventional optical lithography. We demonstrate the broad utility of this method by patterning amorphous and semicrystalline polymers with widely disparate chemical properties, including fluoropolymers, acrylates, carbonates, and olefins. This fiber surface patterning technique enables a unique set of textile functionalities. To demonstrate this, we show microstructured ribbon fibers and fabrics with directional wetting and structural coloration properties.

Figure 1 illustrates the two-step FSP technique. First, macroscale physical material forming techniques are used to generate sub-millimeter class features over a cm^2 class surface area on a bulk, rigid substrate called a preform (Figure 1a–c). Second, the preform is thermally drawn into a flexible fiber device in a process that reduces the preform cross-sectional features down to sub-micrometer, while generating a surface area in the m^2 range (Figure 1d,e). In the first step, we investigated three specific types of physical forming techniques: milling, laser cutting, and molding (Figure S1, Supporting Information). Each method has its unique attributes and is selected based on the properties of the material to be formed. Milling leverages mechanical properties of materials and works well for stiff materials. It can be utilized to define sub-millimeter features with desired depth/width, and can be applied on many common amorphous thermoplastics (e.g., polycarbonate (PC), polytetrafluoroethylene (PTFE), poly(methyl methacrylate)

Dr. T. Khudiyev, Dr. C. Hou, Prof. Y. Fink
Research Laboratory of Electronics
Massachusetts Institute of Technology
Cambridge, MA 02139, USA
E-mail: yoel@mit.edu
Dr. A. M. Stolyarov
MIT Lincoln Laboratory
Lexington, MA 02420, USA
Prof. Y. Fink
Department of Materials Science and Engineering
Massachusetts Institute of Technology
Cambridge, MA 02139, USA
Prof. Y. Fink
Institute of Soldier Nanotechnology
Massachusetts Institute of Technology
Cambridge, MA 02139, USA
Prof. Y. Fink
Department of Electrical Engineering and Computer Science
Massachusetts Institute of Technology
Cambridge, MA 02139, USA

DOI: 10.1002/adma.201605868

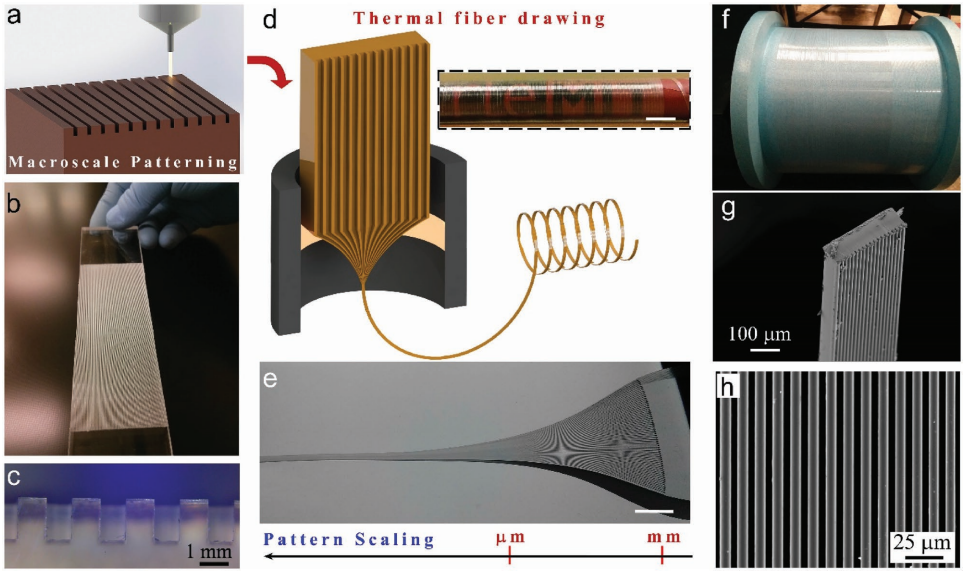

Figure 1. Fiber surface patterning. Fiber drawing technique meets macropatterning technologies. a) Conventional macroscale tools, including milling, laser cutting and molding, are able to process materials at the preform level. b) Image of a PMMA preform patterned by a laser. c) Microscope image of the cross section of a PMMA preform patterned by a 1 mm diameter end mill. d) Thermal fiber drawing reduces the size of the preform as well as the surface patterns. Inset shows several meters of patterned flexible fiber rolled onto a pencil. Scale bar is 5 mm. e) Preform neck obtained after fiber drawing illustrates dimensional scaling of the process. Scale bar is 10 mm. f) Continuous 500 m strands of patterned fiber are displayed on a fiber spool. g) SEM image of a surface-patterned fiber. Fiber thickness and width are < 60 and ≈ 220 μm, respectively. h) SEM image of the gratings on the fiber surface.

(PMMA), etc.) and metals. The laser cutting method leverages optical properties of materials. Most nonmetallic materials are highly absorptive at the CO_2 laser wavelength (10.6 μm), and the cutting process involves three mechanisms: vaporization, melt shearing, or chemical-degradation-based removal of plastic material.[26] Feature sizes obtained using this technique are several hundred micrometers. One of the main advantages of laser cutting is its short processing time. It only takes a few seconds to minutes to create features over the entire preform area. Molding is based on thermal material properties. It relies on shaping surface features of materials by melting or softening them under elevated temperature and pressure. This technique is particularly well-suited for surface patterning semicrystalline polymers such as polyvinylidene fluoride (PVDF). Conventional molding methods for plastics limit the feature sizes to hundreds of micrometers. In the second step, a thermal fiber drawing process is used to scale down the surface pattern of the preform into a flexible surface-patterned fiber (Figure 1d). The preform to fiber draw down ratio (DDR) can range from a factor of ten to several hundred. Critically, the surface-patterned feature size is also reduced by the DDR. The principal challenge in this step is reducing the cross-sectional feature size while mitigating surface energy driven deformation of nonequilibrium surface features, such as rectangular trenches. This is achieved by judiciously controlling the draw temperature, preform feed speed, and fiber draw speed, such that the thermomechanical scale-down process is performed at high stress, where viscous forces dominate and surface-energy-driven deformations are kinetically restrained.[27]

A specific example of a surface-patterned amorphous thermoplastic material produced by the FSP approach is illustrated in the inset of Figure 1d, which shows a piece of meter-long patterned PC fiber rolled onto a pencil. This particular fiber is drawn from a preform with milled surface features. The resulting fiber contains sub-5 μm features in the cross section. Figure 1e shows the neck of the preform transitioning from macro to microscale features. Fiber drawing as a high-throughput process is capable of producing kilometer-long, flexible patterned substrates at speeds of tens of meters per minute (Figure 1f). The final fiber size is several hundred micrometers wide and the feature size on the fiber surface is on the micrometer scale, both of which can be tuned by altering the DDR (Figure 1g,h). The thickness of the fiber is sub-100 μm, which is comparable to a conventional textile fiber size. It is also possible to reduce both width and thickness to sub-100 μm (Figure S2, Supporting Information). See Figure S3 (Supporting Information) for additional examples of patterned amorphous thermoplastics (i.e., PMMA) produced via the laser cutting method.

A particular challenge exists in thermally drawing surface-patterned semicrystalline polymers. Unlike amorphous polymers, which can be drawn at high stress above their glass transition temperature, semicrystalline polymers undergo a rapid drop in viscosity above their melting temperature, significantly complicating efforts of maintaining nonequilibrium surface features during the draw. To address this challenge, we have developed a three-step pattern-transfer approach involving molding and fiber drawing (Figure S4, Supporting Information). First, a film of PVDF is sandwiched and thermally consolidated between two rigid PC plates, one of which is patterned with milling and the other untreated. During consolidation, the PVDF melts and fills the patterns of the PC mold. Second, this sandwiched structure is thermally drawn. During this process, the grating size of the PC mold is reduced and

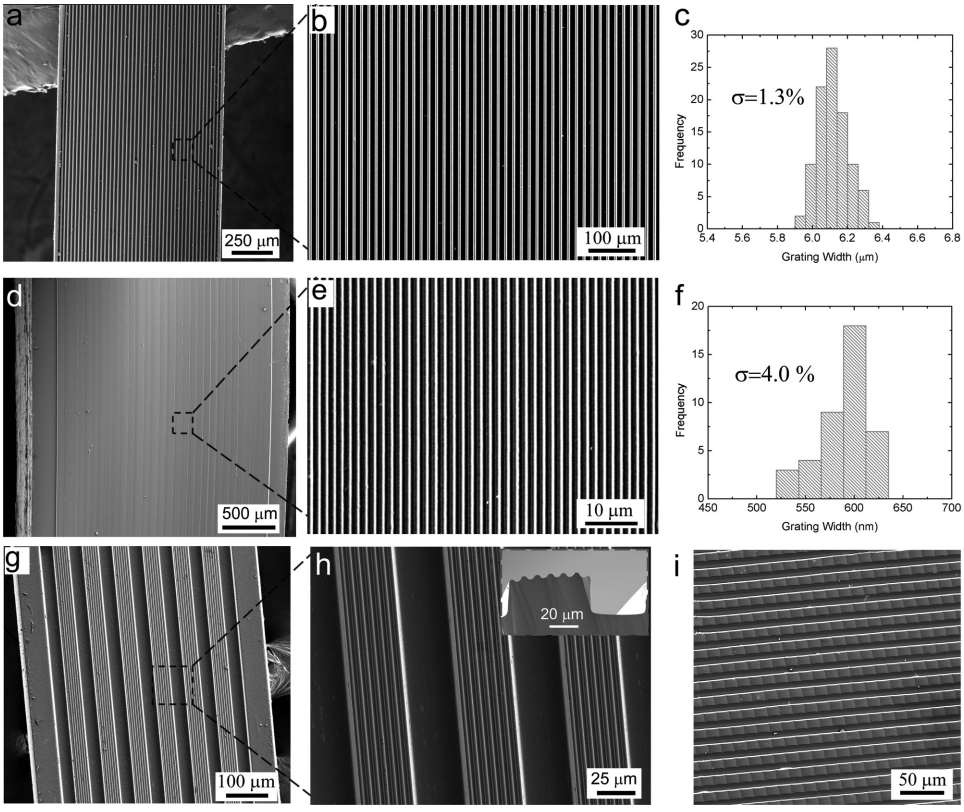

Figure 2. Features of patterned fibers. a,b) SEM image of a surface-patterned fiber after the first draw. c) Statistical distribution of the grating size on the fiber in (a,b) is displayed. Exceptional uniformity of patterns is demonstrated on a 5 m long patterned fiber. Note that the size distribution includes not only axial but also transverse uniformity of the fiber. d) The re-draw approach facilitates reduction of the patterned dimensions to smaller sizes. The fiber after the re-draw process is shown with more than 30 subfibers stacked on the surface. Those subfibers are taken from first draw (a,b) and have microscale patterns on their surface before the re-draw. e) A zoomed-in SEM image shows that the patterns are further reduced to sub-micrometer. f) Statistical distribution of the grating size on the fiber in (d,e) is displayed. Features on the fiber from the first draw are reduced by one order of magnitude, and a grating size of ≈ 600 nm is reached. The sub-micrometer scale patterns also exhibit good uniformity. g,h) Hierarchical complexity can be achieved on flexible polymer fibers. Inset of (h) shows zoomed-in images of two different size scales. i) Post drawing, a stamping process is applied on the fiber surface to generate 2D patterns.

the PVDF liquid follows this size reduction as it is restricted from all sides. While the PVDF is in a low-viscosity state during the draw, the features are maintained due to the highly viscous PC boundaries. The final step involves a simple peeling of the two materials, creating a flexible, surface-patterned PVDF fiber (Figure S4b,c, Supporting Information) (along with a complementary surface-patterned PC fiber). This peeling is facilitated by the low adhesive strength at the PVDF/PC interface. It is worth mentioning that this technique enables sub-micrometer scale surface patterning of semicrystalline materials, with architectural complexity that is difficult to obtain with other techniques.

A unique feature of FSP is that the uniformity of the patterns, both in the axial and transverse directions, is well maintained during the draw, enabling micrometer and sub-micrometer-scale features to extend to kilometer lengths. **Figure 2**a,b depicts an SEM image of a section of fiber which is used for calculating the size distribution of gratings shown in Figure 2c. The standard deviation of the grating width along 5 m of the fiber is as small as ≈ 1%. This fiber contains 40 gratings on the surface and the period is ≈ 24 μm (grating width ≈ 8 μm). The fiber could be further re-drawn to get iterative size reduction of the features, while preserving the uniformity very well (Figure 2d–f). An array of patterned fibers is consolidated on the surface of another preform and then re-drawn, generating fibers with sub-micrometer features (Figure S5, Supporting Information). The standard deviation of the sub-micrometer pillar width is calculated to be ≈ 4%. Note that the grating density (number of periods per unit fiber width) is increased by re-drawing a stacked array of multiple fibers. In particular, a fiber with 1200 periods (period ≈ 1700 nm, where the grating width is ≈ 600 nm) is achieved with a single stack-and-re-draw step. Gratings with feature size down to 200 nm can be achieved under proper draw conditions (see Figures S6 and S7 for details, Supporting Information).

Up to now, we have demonstrated surface patterning of identical, translationally invariant, rectangular sub-micrometer trenches with aspect ratios of the order of 10^{10} (sub-micrometer feature along kilometer-long fiber). While that in itself is unmatched by any other patterning approach, the FSP process presents other unique opportunities for creating surface patterns of significantly higher complexity. First, a structured gradient surface (SGS) can be designed and fabricated (Figure S8, Supporting Information). An SGS refers to a change in either

the periodicity (e.g., a chirped grating) or the depth of a surface feature across or along the fiber surface. Such anisotropic surface features are interesting for a number of emerging research topics, including controlling wettability of surfaces, biomedical applications, and others.[28,29] Second, FSP enables the creation of different cross-section feature profiles. For instance, it is possible to produce high aspect-ratio (Figure S5f, Supporting Information), square, triangular, and hemispherical cross-sectional grating morphologies (Figure S9, Supporting Information). Note that the tapered grating features are of importance for a number of applications, in particular in optics; where a tapered average refractive index profile can significantly reduce surface reflections.[30] Third, FSP can be utilized to fabricate hierarchical surface structures comprising patterns at different length scales. The creation of such structures is known to be very challenging using conventional patterning methods, such as printing or lithography. With FSP, complex hierarchical structures can be generated by using any of the macropatterning techniques, owing to their superior controllability at the macroscale. For example, Figure 2g,h presents hierarchical structures produced by the milling method. The inset shows a single larger period (approximately tens of micrometer wide) with smaller periods (approximately several micrometer wide) on top of it. Finally, longitudinal features can be added to the fiber patterns using a simple stamping technique. To this end, any patterned molds (including a surface-patterned fiber itself) can be used as a stamp. In this study, we use a patterned silicon wafer (Figure S10, Supporting Information) to modify 1D fiber gratings, post draw. The 1D patterned silicon wafer is pressed onto a 1D patterned fiber as the fiber is heated, thus converting a 1D fiber grating into a 2D pattern, as shown in Figure 2i. By adding transverse patterns onto longitudinal features, one can potentially take advantage of 2D structures from their distinct behaviors, in areas such as photonics, surface wetting, electronics, mechanics, etc.

Collectively, these FSP tools enable the exploration of a vast phenomenology and application space. Here, we demonstrate two distinct surface phenomena on surface-patterned fibers: diffraction grating and anisotropic wetting. It is known that light diffracts as it passes through a slit with a size comparable to the wavelength of light. This diffraction effect can be observed via optical gratings on the fiber surface. The experimental setup for measuring the diffraction patterns from the fiber is shown in **Figure 3**a–e. Two fiber samples were measured; one with micrometer-class features and one with sub-micrometer features. The red laser is transmitted through the patterned fiber and the diffraction orders can be clearly observed in the far field. The diffraction angle can be calculated by measuring the distance between these orders. A basic calculation using the diffraction formula $n\lambda = D \sin \alpha$ (where n represents diffraction order, λ is the wavelength of light, α is the diffraction angle for different orders, and D is the period width) confirms that the D values (D_1 = 23.57 µm and D_2 = 1.748 µm) match the measurements from the SEM images (D_1 = 23.67 µm and D_2 = 1.73 µm) of the micrometer and sub-micrometer patterned fibers, respectively, to within 1%. It is apparent, from both the measurement and the calculation, that when the width of the period decreases, the number of supported orders also decreases, and each supported order covers a larger space in the polar domain. This fact, combined with the axial and transverse fiber uniformity, gives rise to observed vivid coloration when the period becomes comparable to visible light wavelengths (i.e., 400–750 nm). Figure 3f–g shows how the fiber exhibits different colors when viewed from different angles. By weaving surface-patterned fibers we demonstrate angle-dependent, chemical-free structural coloration effects over large-area textiles (Figure 3h). An eight-harness satin weave fabric construction was chosen to facilitate maximum fiber-surface exposure.

Surface-patterned fibers present compelling opportunities for all-structural (nonchemical) control of wetting properties. The multichannel, micrometer-to-sub-micrometer scale grating features on the fiber surface induce anisotropic wetting—the wetting behavior is drastically different transverse to the grating pattern, compared to along the fiber axis (Figure 3i). As a control, we first investigate the wetting properties of the bare (nonstructured) side of the fiber. Here, an isotropic contact angle (CA) value of 90° is measured, which is in accordance with the CA value measured on PC slabs prior to drawing, confirming that the drawing process itself does not induce anisotropic wetting. However, when placing a water drop on the patterned surface side, the CA in the transverse direction significantly increases (CA = 148°); while in the longitudinal direction the CA is around 91°, leading to a wetting anisotropy of $\Delta\theta = 57°$. The enhanced hydrophobicity in the transverse direction can be explained by considering the structured surface profile and employing the Cassie–Baxter wetting model.[31] We hypothesize that this model is applicable to our scenario due to the micrometer-sized features of the surface structure, the small ratio between grating width to the period, and the fact that the CA increases beyond 90° for the modified surface. For this type of surface, hydrophobicity is increased due to the trapping of air in the grooves of the grating, thereby increasing the effective interfacial surface energy. It should also be noted that the gratings utilized in this experiment have hemispherical-like edges (which gives even better hydrophobic properties); therefore, a modified Cassie–Baxter model should be used for a more accurate estimation of the CA.[31] The contact angle from this model can be estimated by the following formula:

$$\cos\theta^* = -1 + \phi_B (\cos\theta + 1)^2 \quad (1)$$

where θ is the CA of the bare surface and ϕ_B is the ratio of the grating surface area to the surface area of a period. From the cross-sectional SEM image of the fiber used in the measurement (Figure S4f, Supporting Information), it is estimated that $\phi_B \approx 1/7$ ($\cos\theta = 0$, $\theta = 90°$) resulting in the calculation of $\theta^* \approx 149°$, which matches the experimental result to within 1°.

The anisotropy in the contact angle can be exploited for controlling fluid transport (Figure 3j,k). The potential of anisotropic wetting for facilitating surface-energy-driven fluid flow on the patterned fiber is demonstrated by introducing a flow of fluid onto the surface with the tip of a liquid marker pen. The main carrier solvent used in the ink is isopropanol. Upon touching the patterned surface, the ink from the marker pen preferably flows along the grating axis, while it is restricted along the transverse axis. This enables the simultaneous transport of different fluids on the same fiber surface, as illustrated by flowing different color inks along the fiber without mixing.

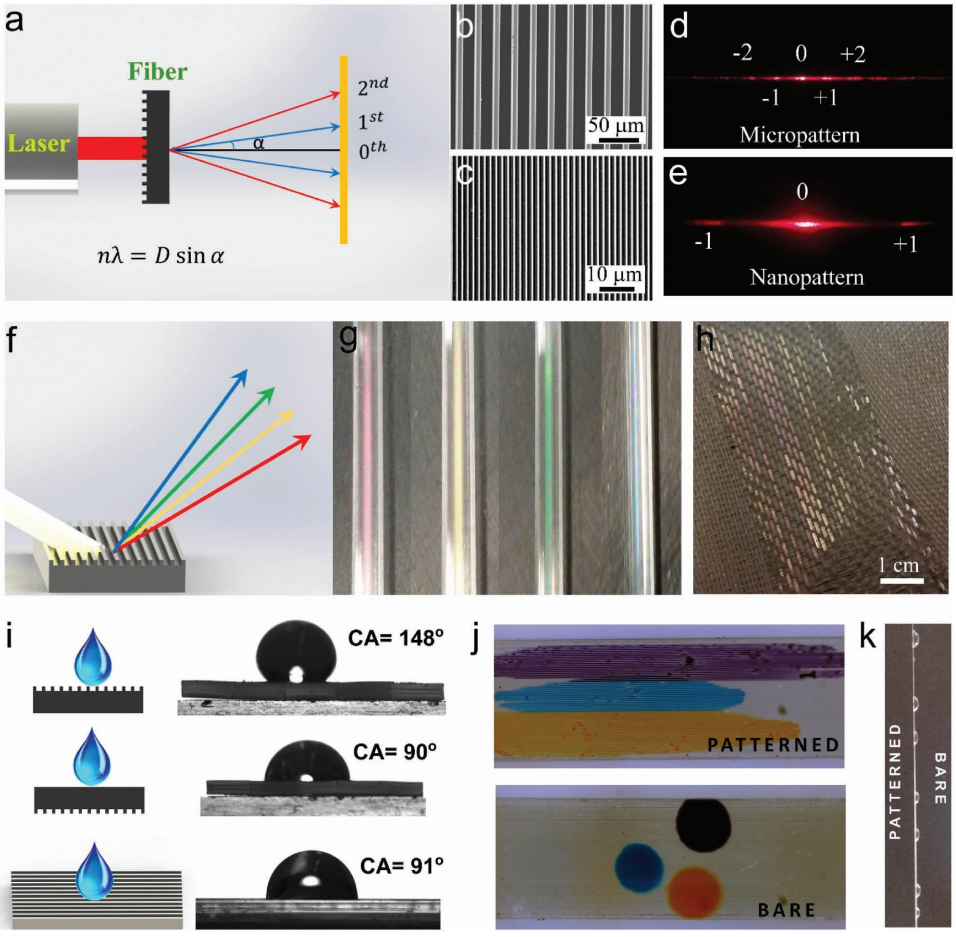

Figure 3. Surface phenomena on patterned fibers and textiles. a) The patterned fiber surface behaves as an optical diffraction grating when the feature size is comparable with visible light wavelengths. A red laser propagates through the gratings and induces separation of diffraction orders in the spatial domain. b–e) The diffraction from the micropatterned fiber has a denser splitting of orders in the polar domain than from the sub-micrometer patterned fiber. f) Schematic illustration of structural coloration on the patterned fiber surface is shown. g) The fiber exhibits different colors when viewed from different angles. h) The surface-patterned fibers are woven into a textile and the textile exhibits large-scale, angle-dependent structural coloration. i) The anisotropic wetting phenomenon is demonstrated on a fiber array (stacks of fibers side-by-side) without any chemical treatment. The micro-patterned fiber surface enhances the hydrophobicity across the patterns (transverse to fiber axis), while the hydrophobicity along the patterned direction (axial) is similar to that of an unstructured surface. j) Liquid ink is placed onto both surfaces of a single fiber that is ≈ 1 mm wide. The ink spreads along the direction of the micro-gratings right after touching the patterned surface (see Videos S1 and S2 in the Supporting Information), while on the bare side it does not have directional preference and hence stays in the local region. k) Water repellency of the patterned fiber surface is demonstrated (Videos S3 and S4, Supporting Information).

As a comparison, the axial flow of the ink is not observed when introducing it to the nonpatterned bare surface (Videos S1 and S2, Supporting Information). Importantly, this demonstrates the ability to achieve directional and confined flow on the surface of individual fibers without employing any chemical treatments. Moreover, the surface-patterned fiber displays water repellency. When the fiber is placed vertically, anisotropic hydrophobicity and gravity facilitate the flow of water along the grating, thus preventing water droplets from staying on the surface. As a comparison, on the nonpatterned side of the fiber, water droplets remain on the surface (Videos S3 and S4, Supporting Information).

To summarize, a novel and effective method of sub-micrometer patterning on flexible polymeric material surfaces is demonstrated. This method is 1) versatile—it can be combined with different surface patterning techniques to treat different types of materials according to their respective properties, and 2) scalable—the thermal drawing process scales down the features of the surface patterns from millimeter to sub-micrometer scale, resulting in kilometer-long, flexible patterned surfaces. The resulting fiber has many potential applications. Two distinct surface phenomena—vivid structural coloration via the diffraction grating effect and anisotropic wetting—have been demonstrated as being enabled by the proposed patterning technique. This fiber surface patterning technique presents vast opportunities in micro/nanofluidics, plasmonic metasurfaces, smart surfaces, organic photonics, biosensors, etc. The synergy of the fiber surface patterning, coupled with in-fiber functional structures, could create more advanced functionalities, paving the way to the development of multifunctional fiber devices and smart textile platforms with increased capabilities.

Supporting Information

Supporting Information is available from the Wiley Online Library or from the author.

Acknowledgements

T.K. and C.H. contributed equally to this work. The authors are grateful to Marty Ellis at Inman Mills for his efforts on weaving the fibers. This work was supported in part by the MIT MRSEC through the MRSEC Program of the National Science Foundation under Award Number DMR-1419807 and was also supported, in part, by the US Army Research Laboratory and the US Army Research Office through the Institute for Soldier Nanotechnologies, under Contract Number W911NF-13-D-0001. This material is based upon work supported by the Assistant Secretary of Defense for Research and Engineering under Air Force Contract Nos. FA8721-05-C-0002 and/or FA8702-15-D-0001. Any opinions, findings, conclusions or recommendations expressed in this material are those of the author(s) and do not necessarily reflect the views of the Assistant Secretary of Defense for Research and Engineering.

Received: October 31, 2016
Revised: December 10, 2016
Published online: March 17, 2017

[1] Industrievereinigung Chemiefaser, Worldwide production volume of chemical and textile fibers from 1975 to 2015 (in 1,000 metric tons).https://www.statista.com/statistics/263154/worldwide-production-volume-of-textile-fibers-since-1975/ (accessed: October 26, 2016).
[2] W. S. Perkins, *Textile Coloration and Finishing*, Carolina Academic Press, Durham, NC **1996**.
[3] W. D. Schindler, P. J. Hauser, *Chemical Finishing of Textiles*, Woodhead Publishing, Boca Raton **2004**.
[4] B. Simoncic, B. Tomsic, *Text. Res. J.* **2010**, *80*, 16.
[5] N. Abidi, L. Cabrales, E. Hequet, *ACS Appl. Mater. Interfaces* **2009**, *1*, 10.
[6] K. L. Hatch, H. I. Maibach, *J. Am. Acad. Dermatol.* **1995**, *32*, 4.
[7] International Agency for Research on Cancer, *Some Flame Retardants and Textile Chemicals, and Exposures in the Textile Manufacturing Industry*, *IARC Monographs on the Evaluation of Carcinogenic Risks to Humans*, Vol. *48*, IARC **1990**.
[8] R. Kant, *Nat. Sci.* **2012**, *4*, 1.
[9] H. M. Pinheiro, E. Touraud, O. Thomas, *Dyes Pigm.* **2004**, *61*, 2.
[10] M. Kobya, E. Demirbas, O. T. Can, M. Bayramoglu, *J. Hazard. Mater.* **2006**, *132*, 2.
[11] K. Lacasse, W. Baumann, *Textile Chemicals: Environmental Data and Facts,* Springer-Verlag, Berlin, Heidelberg **2004**.
[12] A. K. Verma, R. R. Dash, P. Bhunia, *J. Environ. Manage.* **2012**, *93*, 1.
[13] Z. Wang, K. Huang, M. Xue, Z. Liu, *Textile Dyeing Wastewater Treatment*, INTECH Open Access Publisher **2011**, 91–116.
[14] Swedish Chemicals Agency, Chemicals in Textiles: Risks to Human Health and the Environment, Report 6/14, **2014**.
[15] S. Khan, A. Malik, in *Environmental Deterioration and Human Health: Natural and Anthropogenic Determinants* (Eds: A. Malik, E. Grohmann, R. Akhtar), Springer, Dordrecht **2014**.
[16] F. Uddin, *Am. J. Energy Res.* **2014**, *2*, 53.
[17] D. Y. Kim, S. K. Tripathy, L. Li, J. Kumar, *APL* **1995**, *66*, 10.
[18] J. Bico, U. Thiele, D. Quéré, *Colloids Surf., A.* **2002**, *206*, 1.
[19] N. Meinzer, L. B. William, I. R. Hooper, *Nat. Photonics* **2014**, *8*, 12.
[20] R. Gillibert, M. Sarkar, J. F. Bryche, R. Yasukuni, J. Moreau, M. Besbes, G. Barbillon, B. Bartenlian, M. Canva, M. L. de La Chapelle, *Nanotechnology* **2016**, *27*, 11.
[21] S. J. Park, M. L. Seol, S. B. Jeon, D. Kim, D. Lee, Y. K. Choi, *Sci. Rep.* **2015**, *5*, 13866.
[22] Y. Ito, *Biomaterials* **1999**, *20*, 23.
[23] M. Geissler, Y. Xia, *Adv. Mater.* **2004**, *16*, 15.
[24] T. Betancourt, L. Brannon-Peppas, *Int. J. Nanomed.* **2006**, *1*, 4.
[25] A. Yildirim, *Adv. Funct. Mater.* **2014**, *24*, 4569.
[26] *LIA Handbook of Laser Materials Processing* (Eds: J. F. Ready, D. F. Farson), Laser Institute of America,Orlando, FL **2001**.
[27] A. F. Abouraddy, M. Bayindir, G. Benoit, S. D. Hart, K. Kuriki, N. Orf, O. Shapira, F. Sorin, B. Temelkuran, Y. Fink, *Nat. Mater.* **2007**, *6*, 5.
[28] S. Inagi, *Polym. J.* **2016**, *48*, 1.
[29] J. Genzer, *Soft Matter Gradient Surfaces: Methods and Applications*, John Wiley & Sons, Hoboken, NJ **2012**.
[30] B. Daglar, T. Khudiyev, G. B. Demirel, F. Buyukserin, M. Bayindir, *J. Mater. Chem. C* **2013**, *1*, 47.
[31] J. Bico, C. Marzolin, D. Quéré, *EPL* **1999**, *47*, 2.